JOC*Article*

On the Origin of Regio- and Stereoselectivity in the Rhodium-Catalyzed Vinylarenes Hydroboration Reaction

Elias Daura-Oller, Anna M. Segarra, Josep M. Poblet, Carmen Claver, Elena Fernández,* and Carles Bo*

Departament de Química Física i Inorgànica, Universitat Rovira i Virgili, Pl. Imperial Tàrraco 1, 43005 Tarragona, Spain

bo@quimica.urv.es; elenaf@quimica.urv.es

Received September 24, 2003

We studied the hydroboration of vinylarenes using rhodium complexes bearing atropoisomeric ligands. For the first time, an NMR spectroscopy study of the styrene and catecholborane addition to the precursor of catalyst $[Rh(COD)(L-L)]BF_4$, where L−L = (*R*)-BINAP and (*R*)-QUINAP, showed evidence of the structure of intermediates involved in the catalytic cycle. On the basis of this evidence, and using DFT calculations and QM/MM strategies, we investigated the origin of regio- and stereoselectivity. We determined the structure and stability of the key intermediates for several ligands and substrates and found excellent agreement between the relative stability of the intermediates and the experimentally observed trends. Using model systems, we analyzed the role of the steric and electronic features of the ligands and the substrates in detail.

Introduction

The development of asymmetric catalysts for synthesizing added-value reagents is of central importance in modern science and technology.[1] Such asymmetric catalysts are generally transition metal complexes bearing chiral ligands.[2] In homogeneous catalysis, atropoisomeric-type ligands such as binaphthylphosphine (BINAP, Chart 1)[3] are extremely valuable in a number of reactions. Atropoisomers originate from the hindered rotation of the two binaphthyl moieties. Ligands are called homotopic when the two coordinating atoms are equivalent in biphosphine P,P ligands such as BINAP. In heterotopic ligands the atoms are different, as in the case of P,N ligands. Examples of P,N ligands are QUINAP[4] and PYPHOS[5] (Chart 1), which we consider in this study. Although chiral ligands have allowed efficient enantioselective synthesis in several reactions, [1−3] there is no general solution for dealing with asymmetric transformations. Subtle changes in geometry and/or in the electronic properties of ligands and substrates can dramatically affect enantioselectivity.

CHART 1

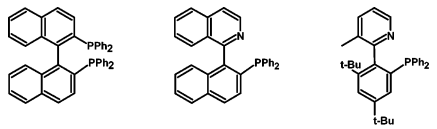

BINAP QUINAP PYPHOS

Although the concepts of chirality content and stereoinduction are clear, several fundamental questions such as how much chirality is involved and how chirality is transferred to the reactive site are largely unsolved. Zhang et al.[6] recently reported how the dihedral angles of chiral biaryl ligands influence the enantioselectivity of the asymmetric hydrogenation reaction. In the asymmetric Diels−Alder reaction of acrylates with cyclopentadiene using homotopic biaryldiol ligands, Harada et al.[7] found that there was a parabolic relationship between the enantiomeric excesses (ee) and the torsion angle of the two biaryl moeties. Lipkowitz et al.[8] defined a measure of chirality content on the basis of continuous chirality metrics (CCM), and when they plotted the ee against CCM, they were able to reproduce exactly the

(1) (a) Kagan, H. B. In *Asymmetric Synthesis*; Morrison, J. D., Ed.; Academic Press: Orlando, FL, 1985; Vol. 5, p 1. (b) Koenig, K. E. In *Asymmetric Synthesis*; Morrison, J. D., Ed.; Academic Press: Orlando, FL, 1985; Vol. 5, p 71. (c) Noyori, R.; Kitamura, M. In *Modern Synthetic Methods*; Schefford, R., Ed.; Springer-Verlag: Berlin, Germany, 1989; Vol. 5, p 115. (d) *Catalytic Asymmetric Synthesis*; Ojima, I., Ed.; VCH Publishers: New York, 2000. (e) Jacobsen, E. N.; Pfaltz, A.; Yamamoto, H., Eds. *Comprehensive Asymmetric Catalysis*; Springer: Berlin, Germany, 1999.

(2) (a) Knowles, W. S.; Christopfel, W. C.; Koenig, K. E.; Hobbs, C. F. In *Catalytic Aspects of Metal Phosphine Complex*; Alyea, E. C., Meek, D. W., Eds.; American Chemical Society: Washington, DC, 1982; p 9325. (b) Kagan, H. B.; Sasaki, M. In *The Chemistry of Organophosphorous Compounds*; Hartley, F. R., Ed.; Wiley: New York, 1990; Vol. 1, p 53. (c) Brunner, H. *Top. Stereochem*. **1998**, *18*, 129.

(3) (a) Miyashita, A.; Yasuda, A.; Takaya, H.; Toriumi, K.; Ito. T.; Souchi, T.; Noyori, R. *J. Am. Chem. Soc*. **1980**, *102*, 7932. (b) Miyashita, A.; Takaya, H.; Toriumi, K.; Souchi, T.; Noyori, R. *Tetrahedron* **1984**, *40*, 1245. (c) Takaya, H.; Mashima, K.; Koyano, K.; Yagi, M.; Kumobayashi, H.; Taketomi, T.; Akutagawa, S.; Noyori, R. *J. Org. Chem*. **1986**, *51*, 629. (d) Takaya, H.; Akutagawa, S.; Noyori, R. *Org. Synth*. **1988**, *67*, 20

(4) Alcock, N. W.; Brown J. M.; Hulmes D. I. *Tetrahedron*: *Asymmetry* **1993**, *4*, 743.

(5) Kwong, F. Y.; Yang, Q.; Mak, T. C. W.; Chan A. S. C.; Chan K. S. *J. Org. Chem*. **2002**, *67*, 2769.

(6) Zhang, Z.; Qian, H.; Longmire, J.; Zhang, X. *J. Org. Chem*. **2000**, *65*, 6223.

(7) Harada, T.; Takeuchi, M.; Hatsuda, M.; Ueda, S.; Oku, A. *Tetrahedorn*: *Asymmetry* **1996**, *7*, 2479.

(8) Gao, D.; Schefzick, S.; Lipkowitz, K. B. *J. Am. Chem. Soc*. **1999**, *121*, 9481.

10.1021/jo035392h CCC: $27.50
Published on Web 03/18/2004

TABLE 1. Influence of the Nature of the Ligand, the Substrate, and the Temperature in the Catalytic Hydroboration/Oxidtion of Vinylarenes with Cationic Rhodium Complexes

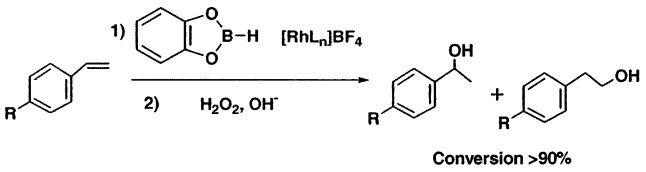

entry	catalytic system	R	*T* (°C)	branched	ee (%)
1	[Rh(COD)(*R*)-BINAP]BF$_4$	H	25	99	57R[a]
2	[Rh(COD)(*R*)-QUINAP]BF$_4$	H	25	98	91.5R[b]
3	[Rh(COD)$_2$]BF$_4$/(*R*)-PYPHOS	H	25	99	69R[c]
4	[Rh(COD)$_2$]BF$_4$/(*R*)-PYPHOS	H	0	99	90R[c]
5	[Rh(COD)(*R*)-QUINAP]BF$_4$	Me	25	98	89R[b]
6	[Rh(COD)(*R*)-QUINAP]BF$_4$	OMe	25	98	94R[b]
7	[Rh(COD)(*R*)-QUINAP]BF$_4$	F	25	98	80R[b]
8	[Rh(COD)(*R*)-QUINAP]BF$_4$	Cl	25	98	78R[b]
9	[Rh(COD)(*R*)-QUINAP]BF$_4$	CF$_3$	25	98	45R[b]

[a] Reference 13a. [b] Reference 14. [c] Reference 5.

same trend as that observed by Harada. By computing the CCM by considering different fragments of a ligand, they introduced the idea of chirafore, which is the part of the molecule responsible for stereoinduction. Lipkowitz et al.[9] recently introduced a new computational mapping technique called stereocartography and demonstrated that efficient catalysts in a Diels−Alder reaction present spatial congruence between the chiraphore and the site where the reaction takes place. In other words, they demonstrated that a stereoselective catalyst is efficient when its maximum ability to differentiate between the two enantiomers occurs in the reaction site, i.e., when the substrate/catalyst interactions are able to discriminate between the reaction pathways leading to one enantiomer and the other. As we will see below, this is also the basic assumption of our study.

The enantioselective synthesis of organoboranes (see Table 1) is an interesting choice in organic synthesis because organoboranes can be converted into a variety of functionalities[10−12] including alcohols, amines, halides, and homologated materials. The fact that the catalytic asymmetric hydroboration reaction of vinylarenes to provide the corresponding chiral 2-aryl boronate esters can occur with regiochemical control and enantiocontrol[13] mainly depends on the structure and electronic nature of the ligand coordinated to the metal in the catalytic complex, the substrate, and the hydroborating reagent.

CHART 2

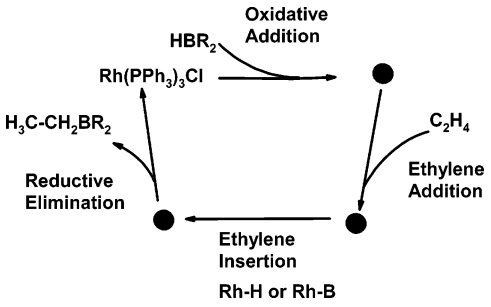

The structure of the ligands and the nature of aryl substituents on the vinylarenes have been experimentally changed to study the relative importance of the steric and electronic effects.[14,15] Also, using catecholborane as the borane source seems to have a beneficial effect on the experimental hydroboration reactions, although it is not yet clear why.

At this stage, we need to consider several points: heterotopic P,N ligands[5,13b,14] modify the rhodium complexes and provide higher enantioselectivities than homotopic P,P ligands[13a] (Table 1, entries 1 and 2); the cationic rhodium complexes modified with heterotopic P−N ligands in the asymmetric induction of the hydroboration of a model vinylarene as styrene are temperature dependent (Table 1, entries 2, 3, and 4); and the electronic nature of the alkenes influences stereoselectivity to the extent that ee values seem to obey a linear free energy relationship with the Hammett constants, (Table 1, entries 5−9).

Therefore, we need to understand the role of the ligands, the substrate, and the hydroborating agent to relieve ligand design from those trial and error approaches and make the performance of the catalytic system more predictable after small variations in the reactants and catalysts.

The nature of the catalytic cycle of alkene hydroboration using the Wilkinson catalyst Rh(PPh$_3$)$_3$Cl, first reported by Mänig and Nöth in 1985,[16] has been addressed experimentally[17−19] and by means of quantum chemistry methods,[20−22] and reviewed recently[23] (Chart 2). The oxidative addition of borane is believed to be the first step followed by the coordination of the alkene, but whether the pathway is associative or dissociative is still controversial. It is worth mentioning that all intermediates involved in the associative pathway have two phosphine ligands in trans disposition, a coordination mode

(9) Lipkowitz, K. B.; D'Hue, C. A.; Sakamoto, T.; Stack, J. N. *J. Am. Chem. Soc.* **2002**, *124*, 14255.
(10) Fu, G. C. In *Transition Metal for Organic Synthesis Building Blocks and Fine Chemicals*; Beller, M., Bolm, C., Eds.; Wiley-VCH: New York, 1998; Vol. 2.
(11) (a) Fernandez, E.; Brown, J. M. In *Modern Amination Methods*; Ricci, A., Ed.; VCH Publishers: New York, 2000. (b) Fernandez, E.; Maeda, K.; Hooper, M. W.; Brown, J. M. *Chem. Eur. J.* **2000**, *6*, 1840. (c) Fernandez, E.; Hooper, M. W.; Knight, F. I.; Brown, J. M. *Chem. Commun.* **1997**, 173.
(12) (a) Chen, A. C.; Ren, L.; Crudden C. M. *Chem Commun.* **1999**, 611. (b) Ren, L.; Crudden, C. M. *Chem Commun.* **2000**, 721.
(13) (a) Hayashi, T.; Matsumoto, Y.; Ito, Y. *Tetrahedron*: *Asymmetry* **1991**, *2*, 601. (b) Brown, J. M.; Hulmes, D. I.; Layzell, T. P. *J. Chem. Soc., Chem. Commun.* **1993**, 1673. (c) Schnyder, A.; Togni, A.; Wiesly, U. *Organometallics* **1997**, *16*, 255. (d) Beletskaya, I.; Pelter, A. *Tetrahedron* **1997**, *53*, 5957. (e) McCarthy, M.; Hooper, M.; Guiry, P. J. *Chem. Commun.* **2000**, 1333. (f) Demay, S.; Volant, F.; Knochel, P. *Angew Chem., Int. Ed.* **2001**, *40*, 1235.
(14) Doucet, H.; Fernandez, E.; Layzell, P. T.; Brown, J. M. *Chem. Eur. J.* **1999**, *5*, 1320.
(15) McCarthy, M.; Guiry, P. J. *Tetrahedron* **2001**, *57*, 3809.
(16) Männig, D.; Nöth, H. *Angew. Chem., Int. Ed. Engl.* **1985**, *24*, 878.
(17) Evans, D. A.; Fu, G. C. *J. Org. Chem.* **1990**, *55*, 2280.
(18) Evans, D. A.; Fu, G. C.; Anderson, B. A. *J. Am. Chem. Soc.* **1992**, *114*, 6679.
(19) Burgess, K.; Donk, W. A. V. D.; Westcott, S. A.; Marder, T. B.; Baker, R. T.; Calabrese, J. C. *J. Am. Chem. Soc.* **1992**, *114*, 9350.
(20) Widauer, C.; Grützmacher, H.; Ziegler, T. *Organometallics* **2000**, *19*, 2097.
(21) Musaev, D. G.; Mebel, A. M.; Morokuma, K. *J. Am. Chem. Soc.* **1994**, *116*, 10693.
(22) Dorigo, A. E.; Schleyer, P. v. R. *Angew. Chem., Int. Ed. Engl.* **1995**, *34*, 115.
(23) Huang, X.; Lin, Z. In *Computational Modeling of Homogeneous Catalysis*; Maseras, F., Lledós, A., Eds.; Kluwer: New York, 2002; p 189.

CHART 3

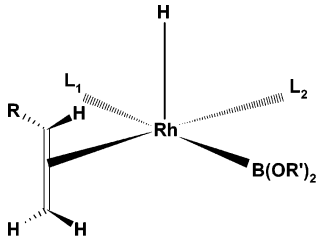

that bidentate ligands such as BINAP or QUINAP, having a narrow bite angle, cannot afford. The dissociative pathway involved pentacoordinated complexes (Chart 3) bearing the chloride (L_1), one phosphine ligand (L_2), the alkene, the hydride, and the BR_2 moiety.

To the best of our knowledge, there have been only a few attempts to rationalize the origin of the regio- and enantioselectivity in hydroboration. One of these was carried out by Brown et al., who proposed as a reactive intermediate a pentacoordinated complex H-Rh-QUINAP-catecholborane-vinylarene, equivalent to the structure shown in Chart 3, (where L_1 and L_2 = QUINAP), on the basis of the X-ray analogue structure from $PdCl_2$-(QUINAP).[24] This model suggests that the electronic effects on enantiomeric excess may arise from the potential π-stacking formed between the aryl group in the substrate and a close aryl group of the ligand. Also very recently, Chan et al.[5] suggested that the electronic effect of modified ligands and/or substrates in asymmetric hydroboration can be explained on the basis of the coordination mode of the vinylarenes to the pentacoordinated H-Rh-(P-N)-catecholborane-vinylarene complexes, which are thought to be the key intermediates. Vinylarenes with electron-releasing substituents may therefore coordinate more strongly trans to the pyridine moiety of the ligand than the vinylarenes with electron-withdrawing substituents. This means that the electron-rich substrates may be closer to the rhodium center than their electron-poor analogues, thus improving stereochemical communication and providing a higher enantioselectivity. In other words, Chan's hypothesis is based on the different interactions between the substrates and the rhodium-ligand-catecholborane complex. However, whether these interactions play the suggested role and are propelled by steric or by electronic effects is still unresolved.

In this paper, we characterized for the first time intermediates involved in the catalytic cycle by means of NMR experiments. Also, using QM/MM strategies, we considered models that mimic the structure of the catalyst as far as possible. We determined the structure and stability of the key intermediates for different ligands and for different substrates and found a very good agreement between the relative stability of the intermediates and the observed trends. Moreover, our model was able to differentiate subtle details such as the ee obtained when similar ligands, such as QUINAP and PYPHOS, were used. However, the main aim of this paper is to thoroughly identify the interactions between the catalyst and the substrate and evaluate the importance of electronic and steric factors in determining regio- and enantioselectivity.

(24) Brown, J. M.; Doucet, H.; Fernandez, E.; Heeres, H. E.; Hooper, M. W.; Hulmes, D. I.; Knight, F. I.; Layzell, T. P.; Lloyd-Jones, G. C. In *Transition Metal Catalysed Reactions*; Murahashi, S. I., Davies S. G., Eds.; Blackwell Science: Oxford, UK, 1999; p 465.

CHART 4

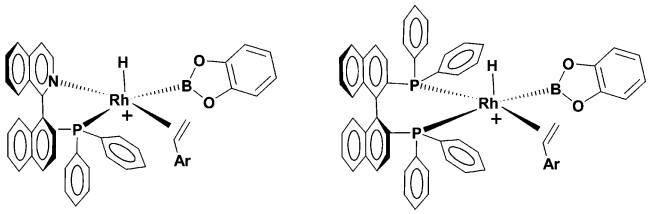

Discussion of Results

1. NMR Characterization of Key Intermediates. To study how specific ligands affect the stereochemistry of the catalytic hydroboration of electronically different vinylarenes, we first need to establish a model for the rhodium intermediate, which is responsible for the diastereoselection. However, although several studies in the literature are related to the isolation of metal-boryl complexes from oxidative addition of R_2BH to metal complexes,[25] very few of them have involved rhodium complexes. The difficulty in isolating rhodium intermediate species in the hydroboration reaction, where the chiral ligand, the hydride, the boryl, and the olefin are coordinated to the metal, has limited the determination of reaction intermediates to comparisons with other metal complexes.[5,14,26] However, these approaches emphasize that the vinylarene substrate coordinates in the chelate ligand−Rh plane, placing the boryl ligand in the same plane and the hydride in the apical position of the pentacoordinated rhodium intermediate. When the chelating ligands are the heterotopic P,N ligands, such as QUINAP and PYPHOS, it is assumed that the boryl ligand is placed trans to the PPh_2 moiety and cis to the pyridine moiety,[5,14] Chart 4.

To help confirm the nature of the key intermediate, we performed an NMR spectroscopy study of the styrene and catecholborane addition to the precursor of catalyst [Rh(COD)(L−L)]BF_4, where L−L = (*R*)-BINAP and (*R*)-QUINAP. For the stoichiometric cis addition of catecholborane and styrene to the [Rh(COD)(BINAP)]BF_4 complex, we can envisage several different isomers (see Scheme 1).

Initially, the ^{1}H NMR spectrum of free catecholborane carried out in CD_3CN showed a quadruplet centered at 4.25 ppm (J_{H-B} = 197.2 Hz), due to the H bonded to B (spin $^3/_2$, 80.4%, natural abundance, spin 3, 19.6%, natural abundance). After the borane reagent and styrene were added to **1**, the resonances of the hydride ligand appeared in an upfield shift centered at δ −14.51 ppm as a double doublet of doublets (see Figure 1). The three coupling constants, J_{H-Rh} = 18 Hz, J_{H-P} = 14 Hz, and J_{H-P} = 9 Hz, are indicative of the hydride position

(25) (a) Hartwig, J. F.; Huber, S. *J. Am. Chem. Soc.* **1993**, *115*, 4908. (b) Nguyen, P.; Blom, H. P.; Westcott, S. A.; Taylor, N. J.; Marder, T. B. *J. Am. Chem. Soc.* **1993**, *115*, 9329. (c) Baker, R. T.; Overnall, D. W.; Harlow, R. L.; Westcott, S. A.; Taylor, N. J.; Marder, T. B. *Organometallics* **1990**, *9*, 3028. (d) Knorr, J. R.; Merola, J. S. *Organometallics* **1990**, *9*, 3008.

(26) Miki, K.; Shiotani, O.; Kai, Y.; Kasai, N.; Kanatani, H.; Kurosawa, H. *Organometallics* **1983**, *2*, 585.

SCHEME 1

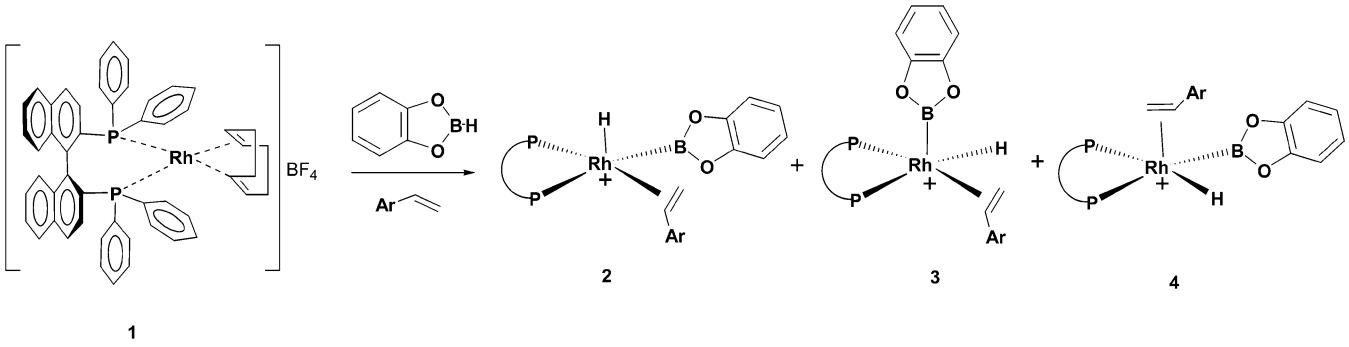

SCHEME 2

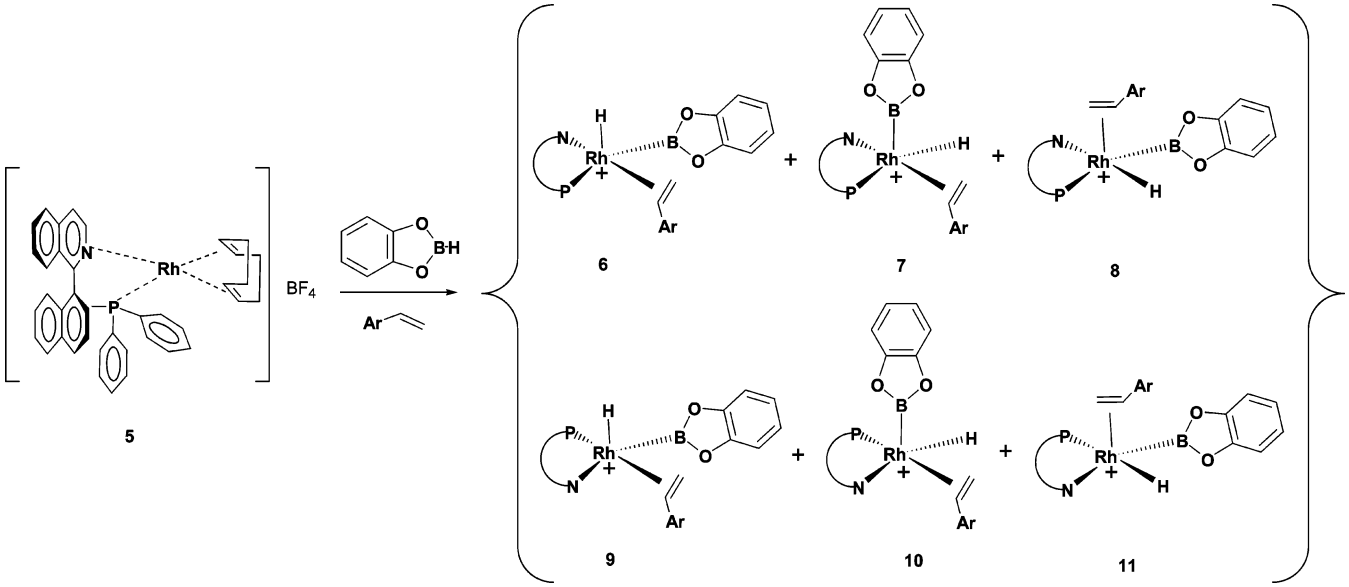

cis to two nonequivalent phosphorus nuclei, which suggests the probable formation of isomer **2**. It is known that the hydride located trans to phosphorus is associated with high coupling constant values ($J_{H-Ptrans}$ = 110−130 Hz). A selective ^{31}P decoupling experiment significantly simplified the hydride signal in the ^{1}H NMR, which showed a broad doublet centered at the same chemical shift δ −14.51 ppm. The inequivalence of the phosphorus nuclei may be due to the fact that while one P is placed trans to the catecholboryl, the other is placed trans to the styrene.

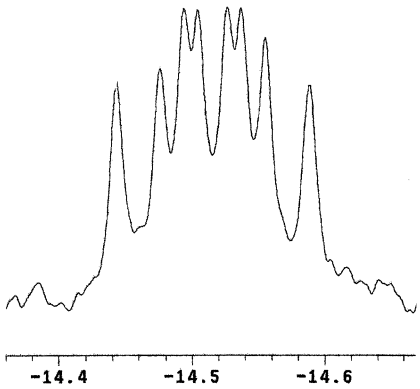

FIGURE 1. Hydride signal in ^{1}H NMR of complex **1** after the addition of catecholborane and styrene.

Confirmation of this arrangement was obtained from ^{11}B NMR, since the initial doublet due to the B bonded to H in free catecholborane (δ 28.88 ppm, J_{B-H} = 197.2 Hz) was shifted as a broad resonance to δ 21.40 ppm after catecholborane and styrene were added to the metal complex. ^{31}P {^{1}H} NMR spectra in d_8-THF also showed a significant shift in the initial doublet centered at δ 26.15 ppm (J_{P-Rh} = 145.5 Hz), from [Rh(COD)(*R*)-BINAP]-BF_4 complex, to two new doublets centered at δ 46.93 ppm (J_{P-Rh} = 207.8 Hz) and δ 46.70 ppm (J_{P-Rh} = 207.8 Hz). Similar resonances have been observed in the literature by monitoring ^{1}H NMR and ^{31}P NMR spectroscopy after catecholborane oxidative addition reaction on IrX(CO)(P−P) (where P−P = dppe, chiraphos).[27] Styrene coordination to rhodium was confirmed by the upfield shift of the alkene hydrogen signals (free styrene δ 5.22, 5.73 ppm; **1** + styrene + catecholborane δ 4.82, 5.43 ppm).

However, from the heterotopic nature of the P,N ligand, the cis addition of catecholborane and styrene on [Rh(COD)(*R*)-QUINAP]BF_4 may involve the formation of a larger number of isomers (see Scheme 2). We tried to monitor the ^{1}H, ^{11}B, and ^{31}P NMR in d_8-THF of the cis addition of catecholborane and styrene on precursor of catalyst **5**, but no hydride signals appeared upfield in the ^{1}H NMR spectra. The most significant features observed

(27) Cleary, B. P.; Eisenberg, R. *Organometallics* **1995**, *14*, 4525.

were, first, the slight shift in the initial doublet in ^{31}P NMR (δ 32.67 ppm, J_{P-Rh} = 140.8 Hz) from [Rh(COD)-(*R*)-QUINAP]BF_4 to upfield (δ 32.25 ppm, J_{P-Rh} = 140.7 Hz) and, second, the displacement of both signals due to H and B nuclei from free catecholborane, which indicates that borane reagent was no longer free. Taking into account recent developments in the literature,[28] we suggested that, alternatively, a three-center bonding interaction between Rh and catecholborane may have taken place.

The difference in behavior between the addition of catecholborane to [Rh(COD)(*R*)-BINAP]BF_4 and to [Rh-(COD)(*R*)-QUINAP]BF_4 may have been due to the basic nature of the ligands and their influence in favoring the oxidative addition in the first case. Although we could not demonstrate the formation of a particular isomer in the cis addition of catecholborane and styrene to [Rh-(COD)(*R*)-QUINAP]BF_4, we assumed that the key intermediate could be any of the isomers **6** and **9**, by similarity with the Rh-BINAP analogue catalytic system. Brown[14] and Chang[5] suggested that the key intermediate is probably **6**.

2. Modeling Strategy. On the basis of these results, we focused on the computational modeling of intermediate type **6** to determine whether this complex could be responsible for diastereoselection or not. The relative position of the alkene substituent in relation to the Rh−H bond defines several isomers, which produce different products each. One could argue that coordination is not necessarily the stereodefining event and rather insertion can be. Evans et al.[17,18] suggested that the migratory insertion of the alkene into the Rh−H bond occurs prior to the reductive C−B bond coupling, but Ziegler's results[20] on model systems for the Wilkinson catalyst suggested that the C−B bond coupling may even be preferred first (see Chart 2). At this point, one must take into account the fact that the reaction is very fast (low barriers, TS reactant-like) and that enantioselectivity is temperature dependent. This led us to assume that the relative stability of the possible isomers was directly related to their population, and that the most stable isomers were those that determined the reaction outcome. Hence, the difference between them arose from the different interactions between the substrate and the catalyst. We think that it does not matter in terms of regioselectivity or enantioselectivity which step occurs first: either insertion of the alkene into the Rh−H bond followed by B−C coupling/reductive elimination or insertion of the alkene into the Rh−B bond followed by H−C coupling/reductive elimination. Instead, the stereochemistry of the final product is probably already determined in the previous intermediate species. For instance, a nonprochiral alkene such as acenaphthene reacts enantioselectively,[14] and as Chart 5 shows, it matters the way the alkene coordinates to the metal (four possibilities in this case). In Chart 5, acenaphthene is coordinated to the H-Rh-QUINAP-catecholboryl complex type **6**, and it is drawn at first plane, occupying a basal position of the square-based pyramid and being the hydride in the apical position (see also Chart 3). Chart 5 shows that each isomer produces a different product, and each isomer presents different interactions between the alkene and the rhodium complex, hence they should exhibit different relative stability. Although this alkene is not prochiral, chirality is induced when the alkene coordinates to the metal complex and insertion takes place. Therefore, we guessed it was plausible that stereodifferentiation originated during alkene coordination and that determining TSs was not necessary in this case. Given the size of the systems and the number of ligands and substrates, a full study of all possible intermediates and TSs is by far beyond the scope of this study.

As we mentioned above, enantioselectivity is highly sensitive to the ligand and to the substrate, so any model that mimics the catalyst as far as possible must take into account all of these features. The difference between the two P,N ligands PYPHOS and QUINAP lies in the ligand backbone, which suggests that steric factors play a role. Recent studies on related topics[29] have shown that the hybrid quantum mechanics/molecular mechanics (QM/MM) IMOMM[30] method is suitable for taking into account the steric effects induced by bulky ligands at a low computational cost. Therefore, we used force field parameters to describe the ligand backbone and the phenyl phosphine substituents. On the other hand, it has been stated that electronic effects are responsible for the different enantioselectivity obtained when substituted styrenes are used. To take into account the electronic effects of styrene substituents, we described the substrate at the QM level. Figure 2 shows the QM/MM partition considered in this study for PYPHOS and QUINAP complexes. For BINAP, we used an equivalent description to the one for the phosphine QUINAP moiety.

This model (see computational details) reproduced the X-ray structure of the square-planar complex $PdCl_2$((*S*)-QUINAP) fairly well.[24] Considering the QM/MM partition for QUINAP and including the Pd and Cl atoms in the QM part, the metal−ligand bond distances computed for $PdCl_2$((*S*)-QUINAP) were in excellent agreement[31] with the X-ray values. Moreover, the ligand conformation was also reproduced. The torsion angle between the two naphthyl moieties was 55.8° whereas the X-ray value was 60.0°. Also the intermolecular $\pi-\pi$ stacking between a phenyl phosphine substituent and the naftyl-pyridine of the QUINAP ligand observed in the X-ray structure was present in the computed structure.[32] This test calculation gave us confidence in the method used. Other authors[33,34] have demonstrated that this methodology is also suitable

(28) (a) Schlecht, S.; Hartwig, J. F. *J. Am. Chem. Soc.* **2000**, *122*, 9435. (b) Hartwig, J. F.; De Gala, S. R. *J. Am. Chem. Soc.* **1994**, *116*, 3661. (c) Baker, R. T.; Ovenall, D. W.; Calabrese, J. C. *J. Am. Chem. Soc.* **1990**, *112*, 9399. (d) Rablen, P. R.; Hartwig, J. F. *J. Am. Chem. Soc.* **1994**, *116*, 4121.

(29) (a) Daura-Oller, E.; Poblet, J. M.; Bo, C. *Dalton Trans.* **2003**, 92. (b) Carbó, J. J.; Maseras, F.; Bo, C.; van Leeuwen, P. W. N. M. *J. Am. Chem. Soc.* **2001**, *123*, 7630. (c) Vázquez, J.; Pericás, M. A.; Maseras, F.; Lledós, A. *J. Org. Chem.* **2000**, *65*, 7303. (d) Ujaque, G.; Maseras, F.; Lledós, A. *J. Am. Chem. Soc.* **1999**, *121*, 1317.

(30) (a) Maseras, F.; Morokuma, K. *J. Comput. Chem.* **1995**, *16*, 1170. (b) Maseras, F. *Chem. Commun.* **2000**, 1821−1827.

(31) Pd−P: 2.22 Å (exptl 2.22 Å). P−N: 2.12 (exptl 2.08 Å). Pd−Cl trans to N: 2.30 Å (exptl 2.27 Å). Pd−Cl trans to P: 2.34 Å (exptl 2.36 Å).

(32) Consider the ring formed by the six carbon atoms of the phenyl phosphine substituent and the pyridine ring. The distance between the two ring centroids is 3.683 Å in the X-ray structure[24] and 3.814 Å in the optimized geometry. The angle between the two rings is 21° in the X-ray structure[24] and 26° in the optimized geometry.

(33) Meyer, E. A.; Castellano, R. K.; Diederich, F. *Angew. Chem., Int. Ed.* **2003**, *42*, 1210−1250 and references therein.

CHART 5

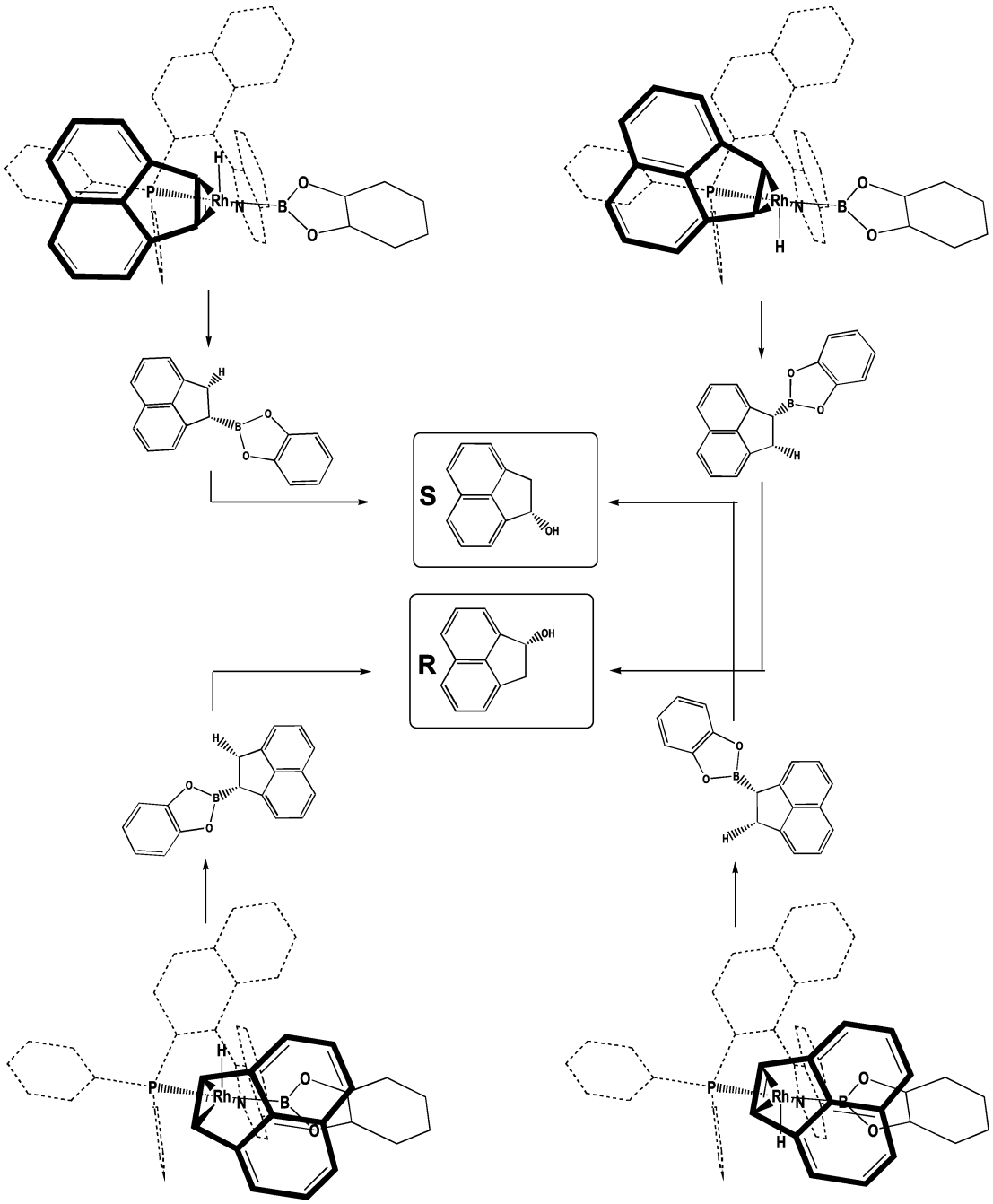

for dealing with transition metal complexes in which $\pi-\pi$ stacking interactions are fundamental.

The key intermediate is therefore considered to be the pentacoordinated H-Rh-(P-N)-catecholborane-styrene complex, which is styrene-coordinated trans to the naftylpyridine moiety and the hydride in axial position (Chart 6). We defined two possible isomers according to the position of the hydride: isomer A has the apex of the square-based pyramid on the up side, see Chart 6, and isomer B has it on the down side. In fact, each isomer presented four possibilities according to the four coordination modes of styrene. In Chart 6, the four coordination modes of a monosubstituted alkene are labeled from A1 to A4. Notice that two of them lead to linear products (A1 and A2 or B3 and B4), one to a branched pro-S product (A3 or B2), and one to a branched pro-R product (A4 or B1). In this study, we determined the relative stability of these eight intermediates for (*R*)-QUINAP, (*R*)-PYPHOS, and (*R*)-BINAP rhodium complexes when *p*-Cl-styrene, styrene, and *p*-OMe-styrene were used as substrates and catecholborane as the hydroborating agent. Full geometry optimizations without constrains were performed for each intermediate, and in all cases, the final geometry showed a coplanar arrangement of the alkene and the Rh−H bond.

3. PYPHOS vs QUINAP. Figure 3 shows the relative stability of the isomeric forms (A1−A4 and B1−B4) for

(34) Magistrato, A.; Pregosin, P. S.; Albinati, A.; Rothlisberger, U. *Organometallics* **2001**, *20*, 4178.

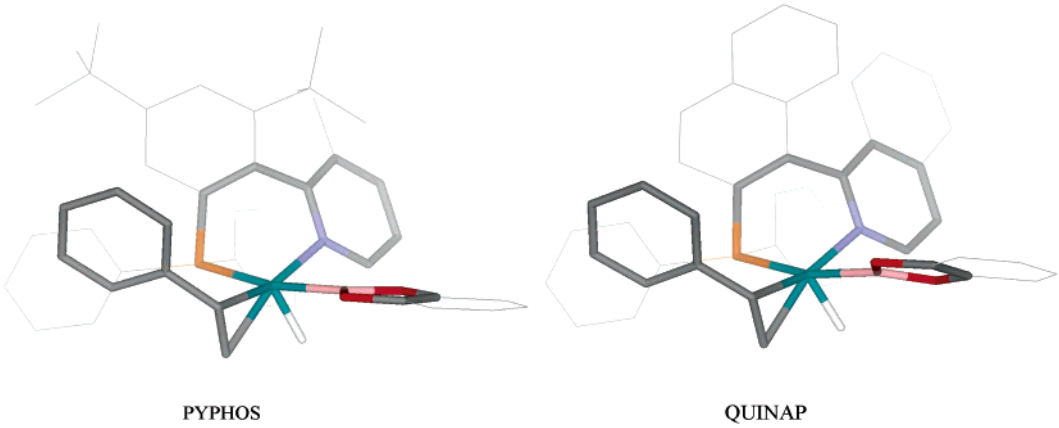

FIGURE 2. Molecular models that illustrate the QM/MM partition used in this study. Atoms treated at the QM level are plotted as colored thick sticks: styrene (gray), Rh (green), H (white), the ligand backbone plus pyridine cycle P (yellow)−N (blue)−C (gray), and catecholboride B (pink) and O (red). Atoms included in the MM part are displayed as thin lines. Hydrogen atoms are omitted for clarity. In the case of BINAP, we used an equivalent partition to that displayed for QUINAP.

CHART 6

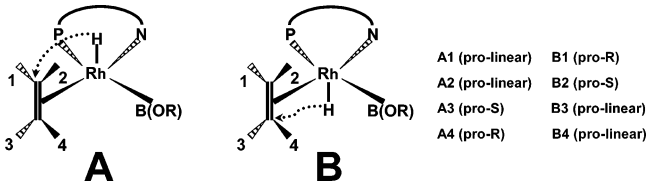

p-Cl-styrene, styrene, and *p*-OMe-styrene with PYPHOS ligand. For styrene, B1 and B2 were the two isomers with the lowest energy, and A2 and A4 were the least stable isomers. In general, the hydride prefers to stay down side, as indicated in Chart 6. For *p*-Cl-styrene and *p*-OMe-styrene the same trend was observed. In all cases, pro-linear intermediates appeared at higher energies than pro-branched intermediates, and pro-R B1 and pro-S B2 were the two most stable forms. The first conclusion to be drawn from these results is that the high regioselectivity observed with this ligand was due to the greater stability of pro-branched intermediates. It is interesting that for QUINAP the same trend was observed. Moreover, the most stable isomer was B1, which was the one that led to the observed product, i.e., R enantiomer. These results fully justify the diastereoselection between pro-R and pro-S intermediates, and show that this differentiation is already present in the key intermediate.

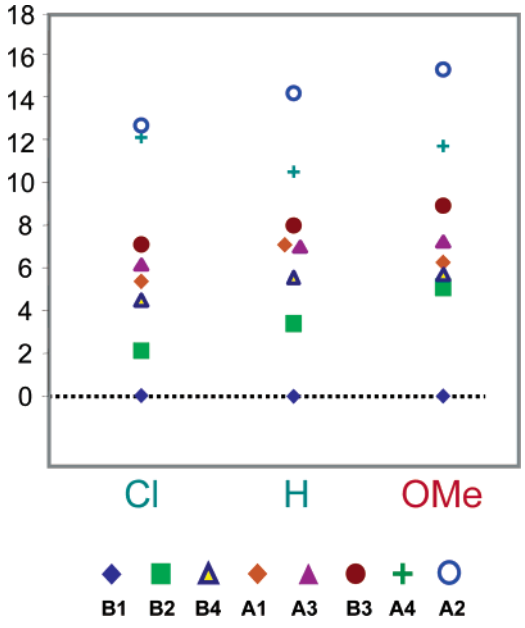

FIGURE 3. Relative energy (kcal·mol^{-1}) of the isomeric forms (A1−A4 and B1−B4) for *p*-chlorostyrene (Cl), styrene (H), and *p*-methoxystyrene (OMe) with PYPHOS.

Note that the difference between pro-R B1 and pro-S B2 isomers, the two most stable forms, increased as the electron-withdrawing character of styrene substituents decreased (Table 2). For PYPHOS, the difference between B1 and B2 increased in the following order: *p*-Cl-styrene (2.1 kcal·mol^{-1}) < styrene (3.5 kcal·mol^{-1}) < *p*-OMe-styrene (5.2 kcal·mol^{-1}). For QUINAP, the difference between B1 and B2 was somewhat greater: *p*-Cl-styrene (2.7 kcal·mol^{-1}) < styrene (4.1 kcal·mol^{-1}) < *p*-OMe-styrene (5.7 kcal·mol^{-1}). For all three substrates, the difference in the relative stability of B1 and B2 increased when we compared PYPHOS and QUINAP. These results may explain the ee values observed in the asymmetric hydroboration when PYPHOS and QUINAP modified cationic rhodium complexes. They may also explain how temperature influences the asymmetric induction. Since the difference between B1 and B2 is greater in QUINAP than in PYPHOS, larger ee values can be obtained at room temperature.

The IMOMM method relies on an additive scheme to compute the total energy of the hybrid QM/MM system. Clearly, the value of each individual component, E_{QM} and E_{MM}, strongly depends on the QM/MM partition, but if this is chosen properly then the energy components provide a useful analysis tool with which to separate and evaluate the electronic and steric effects.[29] We split the computed relative energies into their constituent parts (see Table 2) and observed that in both cases (PYPHOS and QUINAP) the differences in energy between B1 and B2 isomers came mainly from the QM part. Moreover, this contribution, which was almost constant in the two ligands, depended on the substrate: *p*-Cl-styrene (∼1.5 kcal·mol^{-1}), styrene (∼3.0 kcal·mol^{-1}), and *p*-OMe-styrene (∼4,5 kcal·mol^{-1}). However, the MM contribution was different between ligands but remained almost constant among substrates (0.6 kcal·mol^{-1} for PYPHOS

TABLE 2. Relative Energies (kcal·mol^{-1}) and Selected Geometric Parameters (distances in Å and angles in deg) of the Two Most Stable Isomers, B1 and B2, for Different Ligands (PYPHOS and QUINAP) and Different Substrates (*p*-Cl-styrene, styrene and *p*-OMe-styrene)[a]

	PYPHOS						QUINAP					
	p-Cl-styrene		styrene		*p*-OMe-styrene		*p*-Cl-styrene		styrene		*p*-OMe-styrene	
	B1	B2	B1	B2	B1	B2	B1	B2	B1	B2	B1	B2
rel energy	0.0	2.1	0.0	3.5	0.0	5.2	0.0	2.7	0.0	4.1	0.0	5.7
QM contribution	0.0	1.5	0.0	2.9	0.0	4.6	0.0	1.5	0.0	3.0	0.0	4.4
MM contribution	0.0	0.6	0.0	0.6	0.0	0.6	0.0	1.2	0.0	1.1	0.0	1.3
C1−Rh	2.243	2.286	2.252	2.288	2.274	2.295	2.254	2.311	2.258	2.312	2.277	2.330
C2−Rh	2.198	2.204	2.197	2.201	2.186	2.190	2.196	2.198	2.194	2.197	2.190	2.195
C1−C2	1.399	1.400	1.399	1.400	1.402	1.404	1.399	1.400	1.398	1.399	1.401	1.402
Rh−B	2.051	2.046	2.044	2.043	2.044	2.042	2.042	2.038	2.042	2.037	2.066	2.042
Rh−H	1.521	1.527	1.521	1.525	1.521	1.527	1.520	1.532	1.520	1.531	1.523	1.530
P−Rh−N	78.7	79.9	78.3	79.9	78.1	79.8	78.5	79.8	78.4	79.8	78.8	80.3
π3 distance (R1−R2)	8.230	3.919	8.178	3.899	7.008	3.802	8.162	4.018	8.117	3.992	8.032	3.874
π2 distance (R2−R3)	4.022	5.191	4.057	5.118	4.107	5.125	3.530	5.309	3.555	5.265	3.640	5.398
π1 distance (R4−R5)	4.313	4.269	4.277	4.252	4.271	4.254	4.263	4.278	4.253	4.278	4.264	4.296
angle (R1−R2)	59.8	18.5	62.3	23.3	58.9	18.8	47.2	36.8	47.4	36.7	43.4	30.7
angle (R2−R3)	20.0	69.3	22.2	70.6	28.0	68.7	24.4	76.7	24.3	76.4	25.0	76.9
angle (R4−R5)	15.5	12.5	14.5	11.9	13.9	11.7	13.8	11.1	13.3	11.1	12.9	10.1

[a] C1 = alkene terminal carbon; C2 = alkene substututed carbon. R1 = catecholborane; R2 = phenyl styrene; R3 = phenyl P-ligand; R4 = pyridine; R5 = phenyl phosphine.

and 1.2 kcal·mol^{-1} for QUINAP). In other words, and bearing in mind the limitations of this kind of analysis, it seems that when different substrates are considered, the difference in the relative stability of B1 and B2 has a clear electronic origin. If different ligands are considered, the difference arises from the MM contribution and should therefore be assigned to steric effects.

3.1. Structural Analysis of PYPHOS and QUINAP Complexes. Selected geometric parameters shown in Table 2 indicated that the geometry of the intermediates is very similar and that only slight differences are found. In all cases, the terminal alkene carbon (C1) rhodium bond distance was longer than the substituted carbon (C2) rhodium bond. The substituted alkene coordinated to the metal atom in an unsymmetrical fashion, being the terminal carbon tilted away from the metal. For both ligands, the presence of an electron-withdrawing substituent reduced the difference between the two C1−Rh and C2−Rh bonds. However, although the carbon−rhodium bonds showed a variation between the series, the carbon−carbon alkene bond was nonsensitive to the alkene substituent and to the coordination mode. Interestingly, the dihedral angle between the two P- and N-naftyl moieties for the B1 intermediate amounts to 126° for QUINAP and 121° for PHYPHOS.

The analysis of intermolecular interactions is much more significant. In a number of cases intermolecular interactions involving aromatic rings have been identified as key processes in both chemical and biological recognition.[33] Very recently, the role of $\pi-\pi$ stacking interactions in determining the structural features of some palladium complexes using an equivalent method to the one we have used in this study were reported.[34] The latest high-level theoretical results for the benzene dimer[35] identified three main interaction modes: parallel, T-shaped, and slipped-parallel. The modes with the strongest interaction energy were the T-shaped and the slipped-parallel modes[35] (both ca. −2.5 kcal/mol), while the interaction energy in the parallel mode was −1.5 kcal/mol. We analyzed the structures of isomers B1 and B2 in detail and found three $\pi-\pi$ stacking interactions (see Table 2 and Figure 4). Figure 4 refers to QUINAP complexes, but the same can be applied to PYPHOS since both ligands share the same basic structural features. The π1 interaction (Figure 4) is a parallel stacking present in both isomers and corresponds to the interligand phenyl−naphthyl interaction observed in the X-ray[24] and computed structures of $PdCl_2$(QUINAP). In Table 2, π1 corresponds to the distance between rings R4 and R5. Values collected for this parameter showed negligible variation between the series, which indicates that this interaction is always present. In B1-type complexes, we observed a second interaction, named π2, between the substrate and the ligand. This interaction, which must be classified as slipped-parallel, was also observed by Brown et al.[24] Significantly, the distances between the rings involved (R2−R3 distance in Table 2) were around 4 Å in Rh-PYPHOS B1 intermediates and 3.5 Å in Rh-QUINAP B1 intermediates. In B2 complexes, in addition to π1 we observed a new interaction, called π3, between the substrate and catecholborane. In all cases, the distances between these rings (R1−R2 in Table 2) lay in a short range (3.8 to 4.0 Å), and were slightly longer in QUINAP complexes than in PYPHOS complexes. Therefore, the reason for the difference in the relative stability of B1 and B2 complexes might be found in the different interactions between the substrate and the catalyst in each case (the π2 interaction in B1 complexes, and the π3 interaction in B2 complexes).

Moreover, Table 2 shows that these $\pi-\pi$ stacking interactions were sensitive to subtle changes in the substrate and in the ligand. As mentioned above, the main difference between QUINAP and PYPHOS was found in the π2 interaction in B1 complexes. We remind the reader that this kind of interaction is stabilizing[35] and that in the case of the benzene dimer, the equilibrium distance between ring centroids was 3.8 Å. The values in Table 2 (R2−R3 distance) suggest that the greater proximity between the substrate and the rings in QUINAP

(35) Tsuzuki, S.; Honda, K.; Uchimaru, T.; Mikami, M.; Tanabe, K. *J. Am. Chem. Soc.* **2002**, *124*, 104.

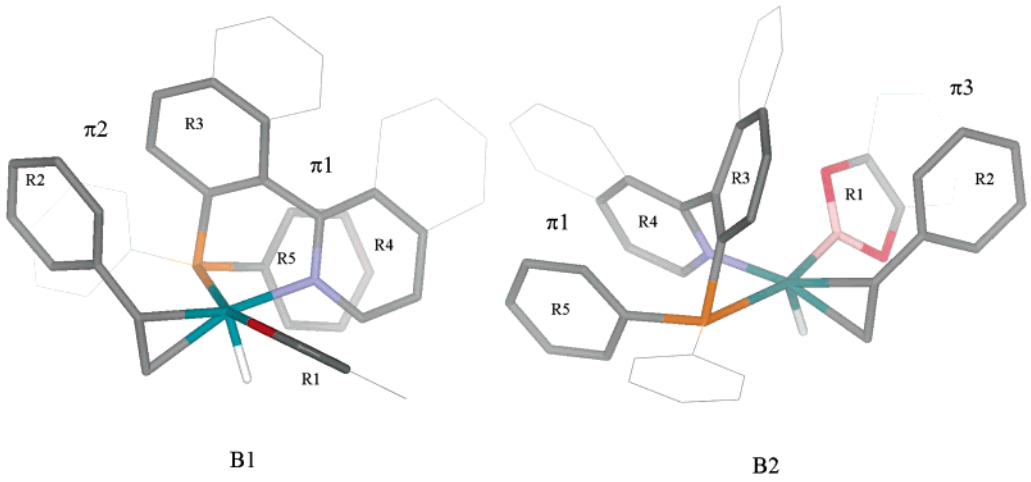

FIGURE 4. $\pi-\pi$ stacking interactions in the QUINAP B1 and B2 isomers. Fragments involved are highlighted. The π1 occurs between a phenyl phosphine (R5, Table 3) and the pyridine ring (R4, Table 3). The π2 is the interaction between the phenyl styrene (R2, Table 3) and the phenyl-P ligand (R3, Table 3), and the π3 corresponds to an interaction between catechoborane (R1, Table 3) and phenyl styrene (R2, Table 3).

than in PYPHOS may be responsible for the enhanced stability of B1 complexes in QUINAP. Enhanced stability refers here to the fact that in QUINAP complexes, the difference between B1 and B2 was greater than that in PYPHOS complexes. We must therefore take into account B2 complexes. The interaction that is present in B2 complexes (π3) was not very different between the QUINAP and PYPHOS complexes, though in the QUINAP complexes it was slightly longer. However, at this point we should consider what kind of interaction π3 is. The B-O_2-C_2 fragment of catecholborane forms the R1 ring (see Figure 4) and it is not clear how this interacts with a phenyl ring. This topic is discussed in the next section, but for now we would like to point out that the main difference in the geometries of the QUINAP and PYPHOS complexes is the $\pi-\pi$ stacking interaction π2.

Also, when the electronic properties of the substrate changed (Cl, H, MeO-styrene), we found clear trends in the $\pi-\pi$ stacking interactions. π2 interaction became less significant when the electron-withdrawing nature of the styrene substituent decreased, while the π3 interaction behaved in the opposite way. The trends were the same for both the QUINAP and PYPHOS complexes.

3.2. Energetic Analysis. To further analyze the role of π2 and π3 interactions in detail, we evaluated the relative strength of each $\pi-\pi$ stacking by considering model systems. Our aim was not to quantitatively evaluate the interaction energy but to study both interactions separately to investigate their relative properties. We built model systems by assembling the two ring moieties, which effectively interacted, as shown in Chart 7, at the same relative orientation as they had in the system as a whole.

Each moiety was treated at the same level as described above (Figure 2). In the case of the π2 interaction, the ligand moiety was modeled by considering a simple phenylphosphine molecule, including the phenyl in the MM part and PH_3 in the QM part. The three substrates (*p*-Cl-styrene, styrene, and *p*-OMe-styrene) were taken into account as themselves and treated at the QM level. Catecholborane, which participates in the π3 interaction, was also included but described by QM/MM as in the whole system (see Figure 1). In this way, we optimized the geometry of the dimers that simulate the π2 and π3 interactions and evaluated the interaction energy (IE) for the three different substrates. Using this strategy we evaluated the electronic effects induced by the substrate on the $\pi-\pi$ stacking interactions.

CHART 7

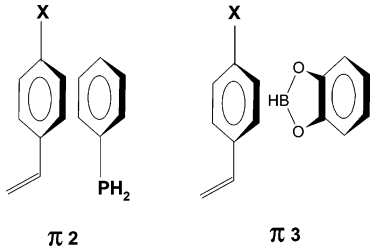

TABLE 3. Interaction Energy (IE in kcal·mol^{-1}), Distance between Ring Centroids (*d* in Å), Angle between Ring Mean Planes (α) for π2 and π3 Interactions in the Model Systems

	π2			π3			
X	IE	*d*	α	IE	*d*	α	IEsp[a]
OMe	−3.9	3.314	9.7	0.2	4.641	17.5	16.3
H	−4.6	3.539	13.3	−0.2	4.525	21.5	15.4
Cl	−5.1	3.375	9.9	−0.7	4.661	18.7	14.2

[a] IEsp corresponds to the interaction energy computed at exactly the same geometry the dimer has in the whole system.

For π2, the interaction energy IE was computed to be negative (Table 3), i.e., there was a stabilizing interaction that increased in the following order: *p*-OMe-styrene < styrene < *p*-Cl-styrene. The distances between the ring centroids (3.4 Å on average) were quite similar to the values computed for B1 complexes in QUINAP. The shorter distance between the ring centroids in the Rh-QUINAP complexes (3.5 Å) than those in the Rh-PYPHOS (4.1 Å) complexes therefore makes the π2 interaction stronger, thus adding stabilization. If we compare QUINAP to PYPHOS, the greater difference in the relative stability of the B1 and B2 complexes may be due to the stabilization of B1 complexes in QUINAP, which is weaker in PYPHOS complexes. Due to the

restricted mobility of styrene coordinated to rhodium and the fact that the two ligands share many structural features, we think that the ligand backbone in QUINAP provides a conformation that enables a greater proximity of the ligand to the substrate, which stabilizes the B1 intermediate more.

We will now analyze the electronic effects induced by the styrene substituents. Both $\pi-\pi$ stacking interactions were affected by changes in the electronic properties of the phenyl ring. In the $\pi 2$ interaction and as stated above, IE increased in the order *p*-OMe-styrene < styrene < *p*-Cl-styrene, which is exactly the opposite order for the relative stability of B1 and B2 intermediates. The properties of the $\pi 3$ interaction were different from those of the $\pi 2$ interaction. Table 3 shows that the IE between styrene and catecholborane was repulsive for *p*-OMe-styrene and somewhat attractive for styrene and *p*-Cl-styrene. However, the equilibrium distance between ring centroids in the model systems (4.6 Å on average) was longer than those in B2 complexes, so we evaluated IE for the $\pi 3$ interaction at the same configuration as that for B2 complexes in QUINAP (IEsp in Table 3). At these shorter distances, the $\pi 3$ interaction was clearly repulsive and increased in the order *p*-OMe-styrene > styrene > *p*-Cl-styrene. We remind the reader that the $\pi 3$ interaction destabilizes the B2 complexes. Though electron-withdrawing substituents increase the attractive strength of the $\pi 2$ interaction and stabilize the B1 complex more, they also decrease the repulsive strength of the $\pi 3$ interaction, thus destabilizing fewer B2 complexes. Electronic effects therefore played opposite roles in terms of increasing the difference in the relative stability of B1 and B2 intermediates. However, if we consider both interactions at the same time, it seems that $\pi 3$ contribute more than $\pi 2$ to the difference between styrene substituents, and to maximizing the destabilization of B2 in *p*-OMe-styrene.

In this section, we identified and analyzed the subtle intermolecular interactions between the substrate, the ligand, and the hydroborating agent. A complex web of $\pi-\pi$ stacking interactions, ligand backbone steric effects, and electronic properties of the substrate affected the relative stability of the key intermediates, therefore stereoselectivity, in a different way. The most stable intermediate B1 was stabilized by an interaction ($\pi 2$) between the substrate and the ligand, while B2 was destabilized by an interaction between the substrate and catecholborane. In this sense, both the ligand and the hydroborating agent were responsible of stereoinduction. This is in complete agreement with our experimental findings. Stereodifferentiation therefore originates at the interaction of these two moieties with the substrate.

4. BINAP. Hydroboration with [Rh(COD)(*R*)-BINAP]-BF_4 produces an ee as low as 57% (Table 1). In this case, if we apply the same hypothesis as for QUINAP and PYPHOS, we would expect the difference in the relative stability of the most stable isomers to be small, even smaller in fact than the lowest value obtained for PYPHOS. In the case of the BINAP complexes and styrene, we considered eight different intermediates, the eight already considered above (Chart 6).

Figure 5 shows one of the minima obtained for the A4 intermediate and the numbering system used to define the different rings. The results are given in Table 4 for isomers whose energy is below a threshold of 3 kcal·mol^{-1}. The most stable isomer was the pro-R intermediate B1, which is in good accord with the experimental findings and our results for the P,N ligands. Moreover, the second most stable was A3, a pro-S intermediate that sits only 0.3 kcal·mol^{-1} above B1. Such a small difference in energy indicates a lower stereodifferentiation, which is in perfect agreement with the low ee obtained when this ligand is used. We found six intermediates above the most stable one, with differences of no more than 3 kcal·mol^{-1}. It is worth mentioning that BINAP complexes

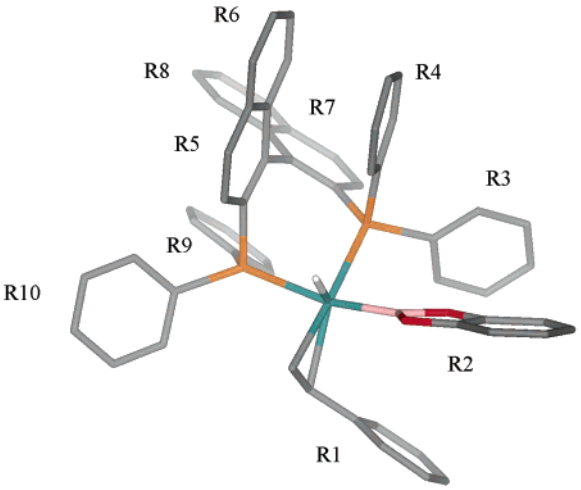

FIGURE 5. Molecular structure of the BINAP A4 complex. Hydrogen atoms are omitted for clarity.

TABLE 4. Relative Energies (kcal·mol^{-1}), Selected Geometric Parameters, Distances between Ring Centroids (Å), and Angles between Rings (Degree) for Some BINAP Complexes

	BINAP					
	B1	A3	A4	B3	B2	A1
product	R	S	R	linear	S	linear
rel energy	0.0	0.3	2.4		2.6	2.7
QM contribution	0.0	−0.3	0.5	1.4	−0.1	3.0
MM contribution	0.0	0.6	1.9	1.0	2.7	−0.3
C1−Rh	2.312	2.352	2.363	2.415	2.303	2.272
C2−Rh	2.269	2.265	2.253	2.268	2.262	2.395
C1−C2	1.391	1.389	1.393	1.388	1.392	1.388
Rh−B	2.054	2.044	2.051	2.066	2.061	2.047
Rh−H	1.523	1.525	1.536	1.547	1.526	1.530
P−Rh−P	86.4	84.7	85.2	84.0	86.0	86.5
distance rings						
1,3						4.614
1,4		4.604		4.587		
1,5	5.171					
1,10	5.342					
2,3	3.999				4.026	
4,5	3.571	3.495	3.487	3.433	3.447	3.764
4,6	3.924	3.949	3.955	3.965	4.004	3.916
7,9	3.629	3.630	3.631	3.573	3.662	3.615
8,9	3.948	3.924	3.954	4.096	3.876	4.040
angle rings						
1,3						8.0
1,4		34.3		31.9		
1,5	61.9					
1,10	37.0					
2,3	36.1				35.1	
4,5	6.1	8.0	6.5	7.7	7.2	5.6
4,6	6.4	7.8	6.4	8.1	7.8	5.0
7,9	7.0	7.3	7.0	7.3	7.4	7.3
8,9	6.8	6.6	6.3	7.3	7.3	6.3

display a number of $\pi-\pi$ stacking interactions. From the distances between ring centroids we clearly identify the interligand (4−5,6) and (9−7,8) stackings also present in X-ray structures[3a,d] of BINAP complexes, substrate−ligand, substrate−catechoborane, and catechoborane−ligand interactions. A detailed analysis of each one is far beyond the scope of this paper, but we should point out that these interactions determine ligand interaction and are also the origin of stereodifferentiation.

Finally, we remind the reader that when we compared the structure of the most stable intermediate for QUINAP and PHYPHOS, we found that the dihedral angle between the P- and N-naphthyl moieties was 126° for QUINAP and 121° for PHYPHOS. In the case of BINAP, we found that the dihedral angle between the naphthyl moieties amounts to 111°. Therefore, a nice correlation appears between the dihedral angle and the ee (QUINAP 88%, PHYPHOS 70%, and BINAP 57%). The larger the dihedral angle, the greater the ee.

Conclusions

An NMR spectroscopy study of the styrene and catecholborane addition to the precursor of catalyst [Rh(COD)(L−L)]BF_4, where L−L = (*R*)-BINAP and (*R*)-QUINAP, showed evidence of the structure of the intermediates that may be involved in the catalytic cycle. From this evidence and using DFT calculations and QM/MM strategies, we studied the origin of regio- and stereoselectivity in the rhodium-catalyzed vinylarenes hydroboration reaction and the role of the steric and electronic features of the ligand and the substrate. The agreement between the results presented in this work and the experimental trends is excellent. For both QUINAP and PYPHOS complexes, pro-R B1 and pro-S B2 were the two most stable forms, and the pro-linear intermediates were the least stable. The results we presented in this paper justify the origin of regioselectivity, but also the origin of enantioselectivity. The difference in the stability of the key intermediates B1 and B2 (Figure 4) when BINAP, QUINAP, and PYPHOS ligands are compared is in perfect agreement with the observed ee values. The greater the difference between B1 and B2, the higher the ee. In this sense, the steric effects induced by the ligand backbone are well reproduced by our models. The same hypothesis explains the effect of temperature on ee. In PYPHOS, because the difference between B1 and B2 is smaller than in QUINAP, a lower temperature is needed to obtain the same ee. It is worth remarking on the correlation found between the ee and the dihedral angle that form the ligand moieties (P−P and P−N). This dihedral angle determines ligand conformation, and this affects the way the alkene substituent interacts with the ligand.

Moreover, the electronic nature of substituted styrenes exerts a subtle influence on enantioselectivity. The observed trends are reproduced by our calculations, and are also reflected in the relative stability of B1 and B2 isomers. By considering model systems, we analyzed the nature of some intermolecular interactions. $\pi-\pi$ stackings played a key role in enantiodifferentiation. Isomer B1 is stabilized because of an attractive interaction (π2) between the ligand and the substrate, while B2 is destabilized due to a repulsive interaction between the substrate and the hydroborating agent. In both cases these $\pi-\pi$ stackings were affected by styrene substituents.

By considering the relative stability of a key intermediate, our computational model reproduced the performance of the catalyst for different ligands and different substrates, and allowed identification of some factors that determine enantiodifferentiation. Although in this study TSs were not determined, the same interactions between the ligand and the alkene would probably be present also in TS structures, thus affecting barriers in the same way. However, the results obtained in this work do not preclude that a more extensive study can modify some conclusion in part. We expect that the conclusions this study rendered will allow the rational optimization of the hydroboration process. Following these results, we are currently doing further research into the role of the hydroborating agent and other ligands, both experimentally and computationally.

Experimental Section

General. Both 300-MHz ^{1}H NMR and 400-MHz ^{1}H NMR spectrometers have been used to analyze the catalytic intermediates. Chemical shifts were reported relative to tetramethylsilane for ^{1}H and ^{13}C, 85% H_3PO_4 for ^{31}P, and BF_3OEt_2 for ^{11}B as the external reference.

Homogeneous Catalytic Hydroboration/Oxidation of Styrene. Styrene (200 μL, 2 mmol) was added to a solution of catalyst (1 mol %, 0.02 mmol, 18 mg L−L = BINAP and 16 mg L−L = QUINAP) in THF (2 mL) under nitrogen. The solution was stirred for 5 min and freshly distilled catecholborane (200 μL, 2 mmol) was then added. The mixture was stirred at ambient temperature for 2 h and then quenched with EtOH (2 mL). Workup must be carried out carefully due to the risk of explosion by using peroxides with ether and THF. Afterward, NaOH (2M, 2 mL) and H_2O_2 (2 mL, 30% v/v) were added and the mixture was stirred for several hours. The reaction mixture was extracted into Et_2O, washed (2 M NaOH, H_2O, saturated brine), and dried over $MgSO_4$, and the products were characterized by chromatography.

Computational Details. DFT calculations were carried out using the Amsterdam density functional program (ADFv2000) developed by Baerends et al.[36,37] The numerical integration scheme used in the calculations was developed by te Velde et al.[38,39] and the geometry optimization algorithms were implemented by Versluis and Ziegler.[40] The electronic configurations of the molecular systems were described by a triple-ζ plus polarization Slater-type basis set, as included in the ADF package (Basis set IV). The 1s−3d electrons for Rh, the 1s electrons for C, B, O, and N, and the 2p electrons for P and Cl were treated as frozen cores. Energy differences were calculated by augmenting the local VWN exchange-correlation potential with nonlocal Becke's exchange-correlation correction[41] and Perdew's correlation corrections[42] (BP86). Relativistic effects were considered using the zeroth-order regular approximation (ZORA).[43] No symmetry constraints were used.

(36) Baerends, E. J.; Ellis, D. E.; Ros, P. *Chem. Phys.* **1973**, *2*, 41.
(37) Fonseca Guerra, C.; Snijders, J. G.; te Velde, G.; Baerends, E. J. *Theor. Chem. Acc.* **1998**, *99*, 391.
(38) te Velde, G.; Baerends, E. J. *J. Comput. Chem.* **1992**, *99*, 84.
(39) Boerrigter, P. M.; te Velde, G.; Baerends, E. J. *Int. J. Quantum Chem.* **1988**, *33*, 87.
(40) Versluis, L.; Ziegler, T. *J. Chem. Phys.* **1988**, *88*, 322.
(41) Becke, A. *Phys. Rev. A* **1988**, *38*, 3098.
(42) (a) Perdew, J. P. *Phys Rev. B* **1986**, *34*, 7406. (b) Perdew, J. P. *Phys Rev. B* **1986**, *33*, 8822.
(43) Van Lenthe, E.; Ehlers, A. E.; Baerends, E. J. *J. Chem. Phys.* **1999**, *110*, 8943 and references therein.

For the QM/MM calculations, we applied the IMOMM method[30] as implemented in the ADF package.[44] The QM level we used was the same as the one in the above paragraph. SYBIL[45] force field was used as implemented in ADF to describe the atoms included in the MM part. For the rhodium and boron atom, we used UFF parameters from the literature.[46] The ratio between the P−C(aromatic) bond distance and the P−H bond distance was 1.234 Å, the ratio between the C(aromatic)−C(aromatic) bond distance and the C−H bond distance was 1.473 Å, and the ratio between the C(aromatic)−C(sp3) bond distance and the C−H bond distance was 1.466 Å.

Acknowledgment. We gratefully acknowledge financial support from the Spanish MCyT under Projects BQU-2002-04110-C02-01 and BQU-2001-0656 and from the CIRIT of the Generalitat de Catalunya under projects SGR-1999-00182 and SGR-2001-00316. We also thank Ramon Guerrero (NMR techniques) and Jose Carlos Ortiz (computational resources).

Supporting Information Available: Computed bonding energies and calculated atomic coordinates for intermediates considered in this study. This material is available free of charge via the Internet at http://pubs.acs.org.

JO035392H

(44) Woo, T. K.; Cavallo, L.; Ziegler, T. *Theor. Chem. Acc.* **1998**, *100*, 307.
(45) Clark, M.; Cramer, R. D., III; van Opdenbosch, N. *J. Comput. Chem.* **1989**, *10*, 982−1012. Singh, U. C.; Kollman, P. A. *J. Comput. Chem.* **1986**, *7*, 718−730.
(46) Rappé, A. K.; Casewit, C. J.; Colwell, K. S.; Goddard, W. A., III; Shiff, W. M. *J. Am. Chem. Soc.* **1992**, *114*, 10024.